SIMULATION ANALYSIS ON THE RISK OF HYDROGEN RELEASES AND COMBUSTION IN SUBSEA TUNNELS

Bie, H.Y.[1] and Hao, Z.R.[2*]
[1] College of Chemistry and Chemical Engineering, Ocean University of China, 238 Songling Road, Qingdao, 266100, China, haiyanbie@ouc.edu.cn
[2] Institute of Oceanographic Instrument of Shandong Academy of Science, 29 Zhejiang Road, Qingdao, 266001, China, haozr001@sina.com

ABSTRACT

Hydrogen is considered to be a very promising potential energy carrier due to its excellent characteristics such as abundant resources, high fuel value, clean and renewable. Its safety features greatly influence the potential use. Several safety problems need to be analyzed before using in transportation industry. With the development of the tunnel transportation technology, the safe use of hydrogen in tunnels will receive a lot of research attentions. In this article, the risk associated with hydrogen release from onboard high-pressure vessels and the induced combustion in tunnels were analyzed using the Partially Averaged Navier-Stokes (PANS) turbulence model. The influences of the tunnel ventilation facilities on the hydrogen flow characteristics and the flammable hydrogen cloud sizes were studied. The tunnel layouts were designed according to the subsea tunnel. And a range of longitudinal ventilation conditions had been considered to investigate the hydrogen releases and the sizes of the flammable hydrogen cloud. Then the hydrogen combustion simulation was carried out after the fixed leaking time. The overpressures induced after the ignition of leaking hydrogen were studied. The influences of ventilation and ignition delay time on the overpressure were also investigated. The main aim was to research the phenomena of hydrogen releases and combustion risk inside subsea tunnels, and to lay the foundation of risk assessment methodology developed for hydrogen energy applications on transportation.

1.0 INTRODUCTION

Hydrogen is considered to be a very promising alternative fuel which is expected to play a significant role in the near future due to its potential to lead to significant reductions in greenhouse gas emissions and improvements in energy efficiency. It is particularly attractive for vehicle applications [1]. The safety of hydrogen automotive applications and the related infrastructure, including garages, maintenance workshops, parking, and tunnels is one area of concern [2].

Schlieren imaging has been used to characterise the shock structures and has shown the axis switching behaviour occurring that is responsible for differences in jet growth rates for the two axes.

When hydrogen is leaking, the hazard is greatly influenced by the dispersion of hydrogen. Many studies have been done on the hydrogen releases in open spaces. Houf et al [3] studied the vertical axisymmetric hydrogen dispersion from an orifice of 1.905mm at a constant mass flow rate. The results showed that the buoyancy had little effects on the jet trajectory and concentration decay when leak densimetric Froude numbers were greater than approximately 500. Takeno et al. [4] experimentally studied the hydrogen leakage diffusion and hydrogen detonation. It was concluded that the explosion power depended on the concentration of hydrogen/air pre-mixture and the turbulence characteristics before ignition. Ruggles and Ekoto [5] studied the effects of nozzle aspect ratio on the under-expanded hydrogen jet release characteristics using schlieren imaging. Under-expanded jets issuing from rectangular nozzles of aspect ratio 2, 4 and 8 were compared to that from 1.5 mm diameter circular nozzle. The results revealed that the axis switching behaviour occurring that is responsible for differences in jet growth rates for the two axes. Olvera [6] analysed the influence of buildings on hydrogen diffusion using the standard $k-\varepsilon$ turbulence model. They concluded that the hazard of indoor hydrogen release was more serious than that of indoor compressed natural gas release. Makarov and Molkov [7] analyzed the structure and behaviour of hydrogen under-expanded jets from plane nozzles and the differences with circular nozzle jets by numerical method. The

simulation results showed that the longest flammable envelope for plane nozzles was shorter than that for circular nozzles for a given surface area. They also studied the under-expanded hydrogen jet fires for plane nozzle AR (Aspect Ratio) =12.8 at 40 MPa. While the systematic study on the effects of nozzle structure on the hydrogen under-expanded hydrogen jet flames was not done.

Once the release occurs in a tunnel, the hydrogen will be trapped inside the tunnel and cause great risk of deflagration and detonation. Many simulation studies have been done on the risk assessment of hydrogen releases in tunnels. Middha [8] carried out CFD simulation study to investigate the risk from hydrogen vehicles in tunnels. It reported a simulation study to examine what is the explosion risk associated with hydrogen vehicles in tunnels. Molkov [9] applied a LES model to study the hydrogen-air deflagrations in a 78.5 m tunnel. They concluded that the overpressure of hydrogen-air deflagration in the tunnel was much larger than that in the open atmosphere. Houf et al. [10] carried out the CFD simulation on the hydrogen releases in tunnels. The results indicated that the potential risk from hydrogen vehicles accidents in tunnels did not significantly increase compared to the individual risk to public from everyday life. Baraldi et al. [11] performed a validation exercise to investigate the accuracy of five CFD codes and their capability of describing hydrogen deflagrations in tunnels. It was found that the experiments and simulations were in good agreement. Tolias et al. [12] also carried out CFD simulations on the hydrogen deflagration in a tunnel. The sensitivity investigation for the parameter of the combustion model illustrated that even small changes can influence the simulation results. And the only significant difference between the LES and RANS models was the arrival time of the pressure peak.

The Partially Averaged Navier-Stokes (PANS) turbulence model was used in our work. Validation simulation experiments were carried out according to the works in Refs. [5]. Then the risk associated with hydrogen releases from high-pressure vessels in tunnels and the induced combustion were analysed using the PANS turbulence model. The main aim was to research the phenomena of hydrogen releases and combustion risk inside highway tunnels, and to lay the foundation of risk assessment methodology developed for hydrogen energy applications on transportation.

2.0 THE SIMULATION METHOD

2.1 Governing equations

The two-equation PANS model is given as [13, 14]:

$$\frac{\partial K_u}{\partial t} + U_j \frac{\partial K_u}{\partial x_j} = P_u - \varepsilon_u + T_{ku} \tag{1}$$

where K_u - RANS kinetic energy; ε_u - kinetic energy dissipation; U_j - the partially averaged velocity; P_u - production of the kinetic energy ($P_u = \tau\left(V_i, V_j\right)\frac{\partial U_i}{\partial x_j}$, $\tau\left(V_i, V_j\right)$ is the generalized central second moment, ***V*** is the instantaneous velocity (subscript *i* and *j* indicating components in different directions)); T_{ku} - transport term ($T_{ku} = \frac{\partial}{\partial x_j}\left(\frac{\upsilon_t}{\sigma_k}\frac{\partial K_u}{\partial x_j}\right)$, σ_k is the corresponding Prandtl number.).

$$\begin{aligned}\frac{\partial \varepsilon_u}{\partial t} + U_j \frac{\partial \varepsilon_u}{\partial x_j} &= C_{\varepsilon 1} f_k \left(\frac{P_u}{f_k} - \frac{\varepsilon_u}{f_\varepsilon f_k}\left(f_\varepsilon - f_k\right)\right)\frac{\varepsilon_u}{K_u} - C_{\varepsilon 2}\frac{f_k}{f_\varepsilon}\frac{{\varepsilon_u}^2}{K_u} + \frac{\partial}{\partial x_j}\left(\frac{\nu_i}{\sigma_\varepsilon}\frac{\partial \varepsilon_u}{\partial x_j}\right) + \left(U_j - \overline{U_j}\right)\frac{\partial \varepsilon_u}{\partial x_j} \\ &= C_{\varepsilon 1}\frac{P_u \varepsilon_u}{K_u} - C_{\varepsilon 2}^{*}\frac{{\varepsilon_u}^2}{K_u} + \frac{\partial}{\partial x_j}\left(\frac{\nu_u}{\sigma_{\varepsilon u}}\frac{\partial \varepsilon_u}{\partial x_j}\right)\end{aligned} \tag{2}$$

where $C_{\varepsilon 1}$, $C_{\varepsilon 2}$ - model coefficients; f_k, f_ε - unresolved kinetic energy and unresolved dissipation; $C_{\varepsilon 2}{}^{*} \equiv C_{\varepsilon 1} + \frac{f_k}{f_\varepsilon}\left(C_{\varepsilon 2} - C_{\varepsilon 1}\right)$; $\sigma_{\varepsilon u} \equiv \sigma_\varepsilon \frac{f_k{}^2}{f_\varepsilon}$ - high Reynolds number flow; $\sigma_{\varepsilon u} \equiv \sigma_\varepsilon$ - low Reynolds number flow.

The mass conservation equation [15]:

$$\frac{\partial \rho}{\partial t} + \frac{\partial \rho u_j}{\partial x_j} = 0 \tag{3}$$

The momentum conservation equation [15]:

$$\frac{\partial(\rho u_i)}{\partial t} + \frac{\partial(\rho u_i u_j)}{\partial x_j} = -\frac{\partial p}{\partial x_i} + \frac{\partial}{\partial x_j}[\mu(\frac{\partial u_i}{\partial x_j} + \frac{\partial u_j}{\partial x_i})] - \frac{2}{3}\frac{\partial}{\partial x_i}\left[\delta_{ij}\left(\rho k + \mu \frac{\partial u_k}{\partial x_k}\right)\right] \tag{4}$$

where k - the kinetic energy and μ - the dynamic viscosity.

The energy conservation equation [15]:

$$\frac{\partial}{\partial t}\left(\rho E\right) + \frac{\partial}{\partial x_i}\left[u_i\left(\rho E + p\right)\right] = \frac{\partial}{\partial x_j}\left(k_{\text{eff}}\frac{\partial T}{\partial x_j} + u_i\left(\tau_{ij}\right)_{\text{eff}}\right) + S_h \tag{5}$$

where ρ - density; E - total energy; T – temperature; k_{eff} - effective thermal conductivity; $\left(\tau_{ij}\right)_{\text{eff}}$ - the deviatoric stress tensor defined as $(\tau_{ij})_{\text{eff}} = \mu_{\text{eff}}\left(\frac{\partial u_j}{\partial x_i} + \frac{\partial u_i}{\partial x_j}\right) - \frac{2}{3}\mu_{\text{eff}}\frac{\partial u_i}{\partial x_i}\delta_{ij}$, and μ_{eff} is the effective dynamic viscosity; S_h - effect of enthalpy transport caused by species diffusion.

The species conservation equation:

$$\frac{\partial}{\partial t}(\rho Y_i) + \nabla \cdot (\rho \vec{v} Y_i) = -\nabla \cdot \vec{J}_i + R_{i,r} \tag{6}$$

where $R_{i,r}$ - net rate of production of species i by chemical reaction r; $\vec{J}_i$ - diffusion flux of species i. $R_{i,r}$ is given by the smaller of the two expressions below:

$$R_{i,r} = v'_{i,r} M_{w,i} \mathrm{A} \rho \frac{\omega}{k} \min_{\mathrm{R}}\left(\frac{Y_{\mathrm{R}}}{v'_{\mathrm{R},r} M_{w,\mathrm{R}}}\right) \tag{7}$$

$$R_{i,r} = v'_{i,r} M_{w,i} \mathrm{AB} \rho \frac{\omega}{k} \frac{\sum_P Y_P}{\sum_j^N v''_{j,r} M_{w,j}} \tag{8}$$

where Y_P - mass fraction of any product species P; Y_R - mass fraction of a particular reactant R; $M_{w,i}$ - molecular weight of species i; A, B - empirical constants, A=4.0 and B=0.5. Once the flame is ignited, the dissipation rate of the eddy is usually smaller than the Arrhenius rate, and thus the reactions are mixing-limited.

$\vec{J}_i$ is given by:

$$\vec{J}_i = -\left(\rho D_{i,m} + \frac{\mu_t}{S_{c_t}}\right)\nabla Y_i \tag{9}$$

where $D_{i,m}$ - diffusion coefficient for species i in the mixture; μ_t - turbulent viscosity; S_{c_t} - turbulent Schmidt number.

2.2 Validation of the model

2.2.1 Details of the validation simulation model

To prove that the PANS model is pertinent for the simulation of high-pressure hydrogen release, simulations were carried out based on the works of [5] using FLUENT. The calculation domain is shown in Fig.1. The diameter of the circular nozzle was d = 1.5 mm. A cylinder was established representing the internal part of the nozzle which is not clearly visible in the model due to its relatively small size. The cylinder was used to generate a realistic flow field at the nozzle exit. The external jet flow field was a frustum with a base diameter of 1,500 mm, an outer diameter of 5,000 mm, and a height of 7,000 mm. The calculation domain was meshed using structured grids, and the grids in the core regions of the hydrogen release and combustion were refined. The total grid number was 779,585.

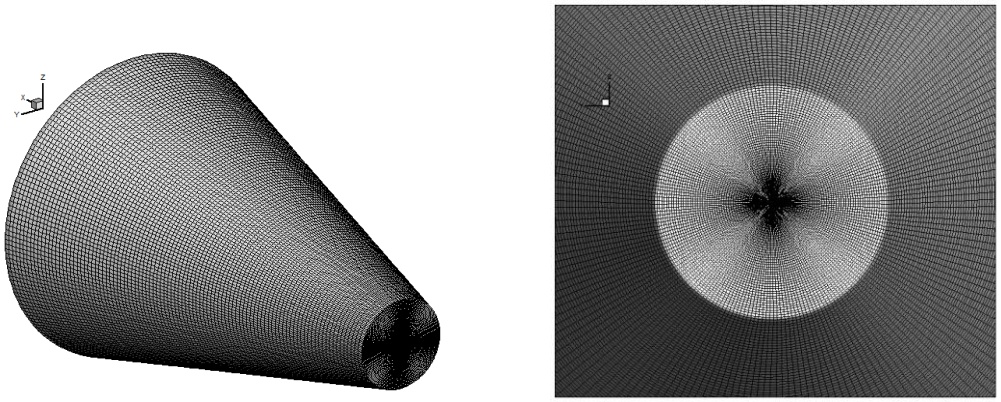

(a) Computational domain (b) Grids cross section at x = 0

Figure 1. The validation simulation model

The inlet of hydrogen at the open exit of the cylinder was a pressure inflow boundary and the outlet of the air a pressure outflow boundary. The cylinder walls were set to be the solid wall. The base of the frustum was set to the solid wall condition, and the frustum sides and outer boundary were set to the pressure outlet condition.

The SIMPLE algorithm was employed to implement the coupled solution of pressure and velocity fields. The time step was Δt = 0.005 s in order to ensure that the calculation could be implemented.

2.2.2 Comparison of the simulation results and experimental results

Fig. 2 shows the predicted velocity vectors and the experimental results by Ruggels and Ekoto [5] at p = 1MPa. It can be seen that a supersonic jet was generated at the nozzle and the classical barrel shock, Mach disk and outer compression waves could be seen clearly. The simulated Mach disk was about 3.3 mm away from the nozzle and the diameter was about 1.4 mm. While the experimental results were 3.05 mm and 1.3 mm respectively. And the shape of the reflected shock structure presented in the downstream of Mach disk was like a diamond which was in good agreement with the experimental results.

Fig. 3 showed the radial profiles of the mean mass fraction, Y_{H2}, of the circular nozzle at 1 MPa for the distances of y/D = 30 and 150. It can be seen that both profiles are of the Gaussian type. In order to analyse the jet characteristics, the normalized mean concentration profiles at pressures of 10 MPa and 20 MPa were given in Fig. 4. The experimental results and simulation results using LES model carried out by Chernyavsky [16] were also given in the figure. It indicated the self - similar collapse of the hydrogen mass fraction profiles normalized by jet half - width L_y. And the hydrogen mass fraction profiles deviated from the Gaussian distribution, near the jet-ambient air interface, indicating potentially higher mixing and therefore more air entrainment. It was in good agreement with the conclusions of [16]. Therefore, the PANS model showed high precision in the simulation of high pressure ratio and high velocity hydrogen jet.

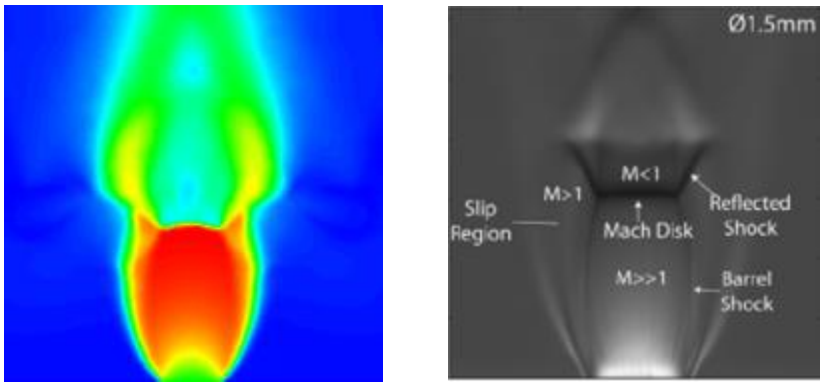

Fig. 2 The under-expanded jet and downstream shock structure of D = 1.5mm

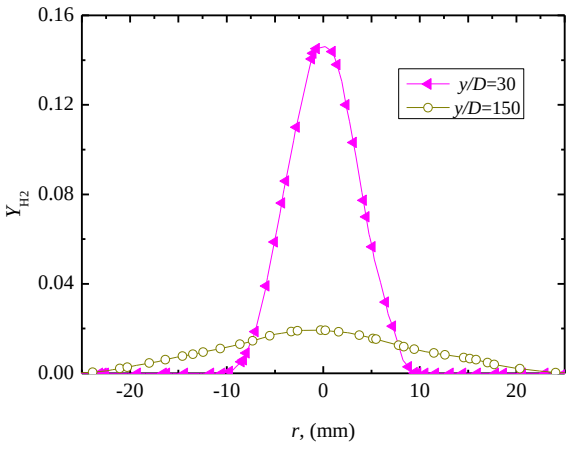

Fig. 3 Radial profiles of the mean mass fraction of circular nozzle at 1MPa

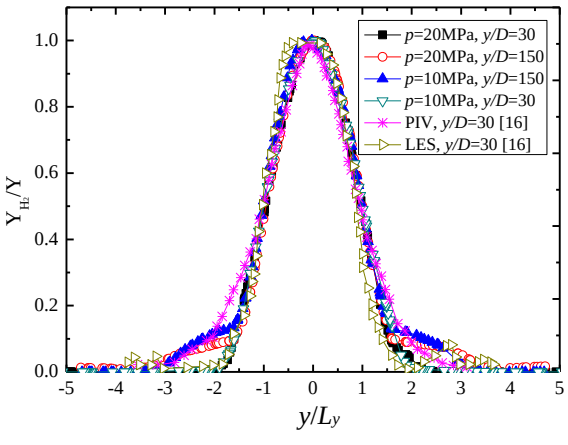

Figure 4. Normalized mean concentration profiles of circular nozzle at different pressures

3.0 NUMERICAL DETAILS

The geometry model for the simulation of the hydrogen releases and combustion was proposed according to the Kiaochow Bay subsea tunnel which is three-lane highway, as shown in Fig. 5. The length of the tunnel in the model was set to be 500 m, the width of the tunnel was 13.5m and the high of the tunnel was 5m. The sectional view of the tunnel model was shown in Fig. 6. All releases were assumed to be upward and therefore only one vehicle was considered in this model. The $L \times W \times H$ of the hydrogen leaking vehicle was 4.7m×1.8m×1.5m according to a typical mid-sized vehicle. The compressed hydrogen gas vehicle loaded 4.955 kg H_2 stored in a 150L cylinder at a storage pressure of 70 MPa. The cylinder was represented as a simple rectangular block (1.0m×0.5m×0.3m) located in the car trunk. The H_2 release was assumed to be due to the activation of a pressure relief device (PRD), so that the entire contents of the cylinder were released to the atmosphere. And the nozzle of the PRD was set to be 6 mm which was consistent with the earlier study [17].

The calculation domain was meshed using tetrahedral grid, and the grids in the core regions of the hydrogen release and combustion were refined. The total grid number was 473,935. Ambient condition of 1 bar pressure and 20 ℃ temperature were used in this model. Four ventilation conditions were proposed: 0m/s, 1m/s, 3m/s and 6m/s. Five monitoring points were set in the model, as shown in Fig. 5. P1 was arranged 5 m away from the leakage location along the direction of traffic, P2 was arranged 10 m away from the leakage location along the direction of traffic, P3 was arranged 5 m away from the leakage location in the inverse direction of vehicle, P4 was arranged 10 m away from the leakage location in the inverse direction of vehicle and P5 was arranged 5 m horizontally away from the leakage location and 0.2 m from the ceiling of the tunnel.

The dispersion simulations were carried out firstly for the fixed time. Then the ignition of the hydrogen cloud was adopted 3.1 s or 6.1 s after the leakage of hydrogen.

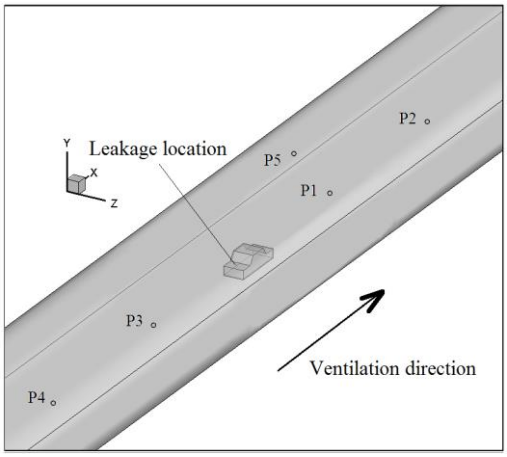

Figure 5. Partial view of the model

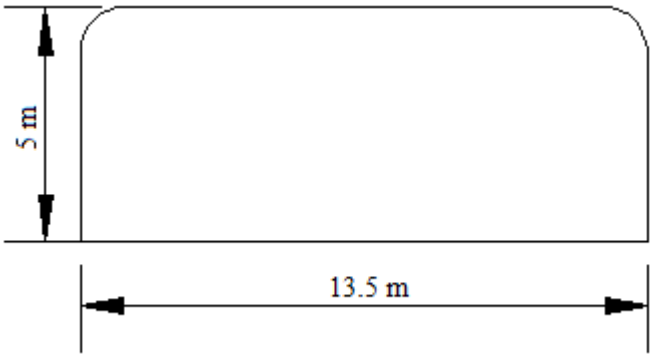

Figure 6. Sectional view of the tunnel

4.0 SIMULATION RESULTS AND ANALYSIS

4.1 Characteristics of hydrogen dispersion

When the hydrogen stored in the 70MPa hydrogen cylinder released, a supersonic jet would be generated and quickly reached to the top of the tunnel, and then rapidly diffused. Fig. 7 showed the longitudinal hydrogen concentration contours along the tunnel axis at t=3s under different ventilation conditions. It can be seen that the flammable hydrogen cloud was several metres long in 3s. When the ventilation velocity was 1m/s, the hydrogen cloud in the downstream was significantly smaller than that in the upstream. As the ventilation velocity increased, the flammable hydrogen cloud in the

upstream decreased. Fig. 7 (d) illustrated that when the ventilation velocity was 6m/s, the high hydrogen concentration (larger than 10%) was much smaller than that of the 0 m/s ventilation velocity.

Fig. 8 showed the vertical hydrogen concentration contours through the plane perpendicular to the axis of the tunnel at *t*=3s under different ventilation conditions. The released hydrogen jetted to the ceiling of the tunnel and then spread down along the wall due to the limited space. It can be seen that the flammable hydrogen cloud was very close to the ground. The presence of tunnel ventilation reduced the risk of hydrogen release on the region near the ground. As the ventilation velocity increased from 0m/s to 6m/s, the range of hydrogen distribution decreased obviously.

Therefore, it can be concluded that ventilation can greatly influence the distribution of hydrogen when hydrogen released from the PRDs. The upstream of the ventilation was less hazardous than the downstream and the risk around the hydrogen leaking vehicle was reduced significantly. According to the simulation results, the tunnel is advised to be ventilated in the same direction as the road traffic. Thus, once the hydrogen was released, the hydrogen would disperse along the ventilation. Although the road vehicles in the downstream of the ventilation were more dangerous, they were much more convenient to drive away from the accidental scene. And people in the vehicles blocked in the upstream would have more time to escape.

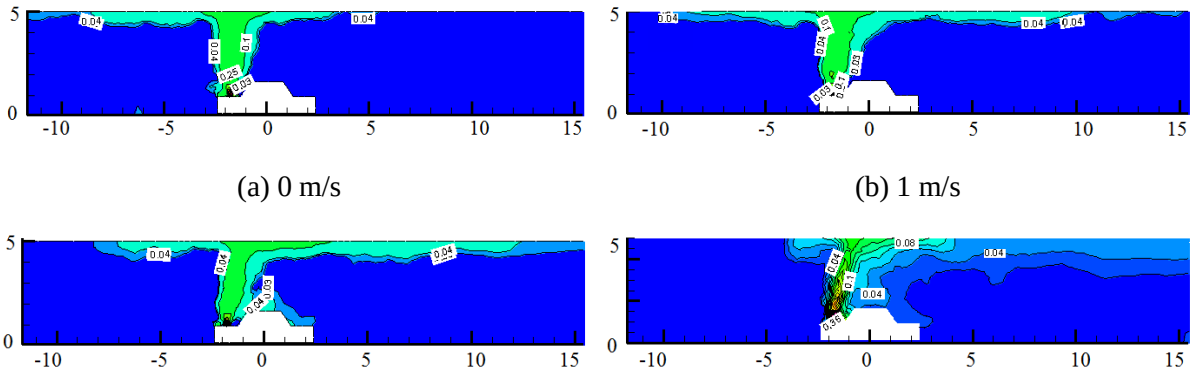

(a) 0 m/s (b) 1 m/s

(c) 3 m/s (d) 6m/s

Figure 7. Longitudinal hydrogen concentration contours along the tunnel axis at *t*=3s

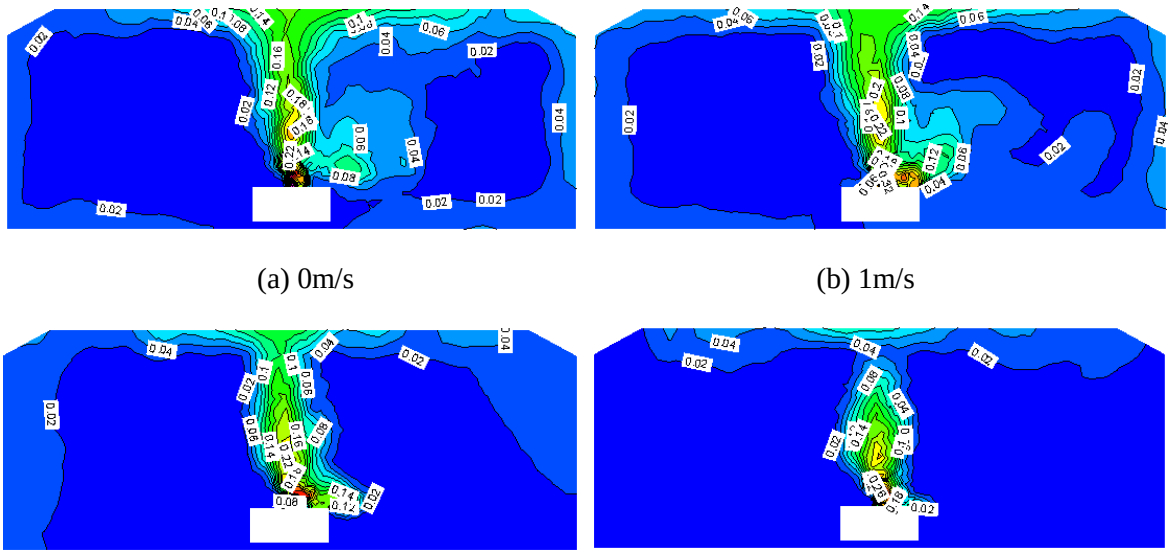

(a) 0m/s (b) 1m/s

(c) 3m/s (d) 6m/s

Figure 8. Vertical hydrogen concentration contours through the plane perpendicular to the axis of the tunnel at *t*=3s

Fig. 9 shows the time evolution of predicted H_2 mole fraction of P5 under different ventilation conditions. Without ventilation, the predicted hydrogen mole fraction increased rapidly from 0 to approximately 0.015 around 4.2 s of the start of the release at P5 (5 m along the tunnel axis from the leakage location). And then the hydrogen mole fraction reached to a peak of 0.025 at about 5.2s after the start of the release. When the ventilation velocity was up to 1m/s, the predicted H_2 mole fraction increased from 0 to 0.035 at about 2.6s after the start of the release. With the increasing of ventilation, there was a less delay before the detection of hydrogen and the magnitude of the hydrogen mole fraction increased. This was because more hydrogen was carried downstream by the ventilation.

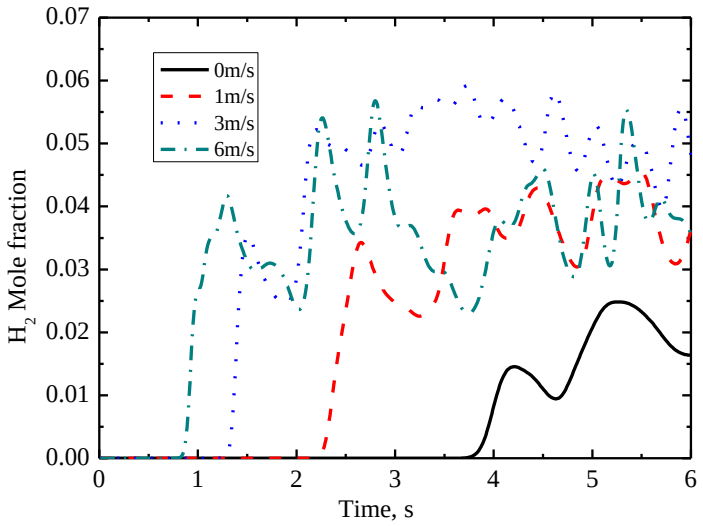

Figure 9. Time evolution of predicted H_2 mole fraction of P5

4.2 Overpressure after ignition

The comparison of the overpressure history of the four monitoring points (P1, P2, P3, P4) when the hydrogen cloud was ignited 3.1s after the beginning of release was shown in Fig. 10. When the ventilation was 0m/s, there was little difference in the overpressures between the points with the same distance from the leaking location (P1 and P3, P2 and P4). At larger distances from the release, there was a longer delay before the detection of the overpressure and the magnitude was reduced, which was in agreement with the distribution of H_2 mole fraction as mentioned above. In order to study the influence of ventilation on the overpressures, the overpressure history of the monitoring points with 6 m/s ventilation was given for comparison. It can be seen that the rapid rising time of overpressure in the upstream (P3 and P4) was slightly later than that in the downstream (P1 and P2) with ventilation. It should be pointed out that the maximum overpressures of P3 and P4 were lower than those of P1 and P2 due to the ventilation. When the ventilation was 6m/s, the overpressure of P1 increased compared to that when the ventilation was 0m/s. The overpressure decreased when the ventilation velocity increased from 0m/s to 6m/s. Both the growth rate of the overpressure after ignition and the attenuation rate after reaching the peak decreased with the increasing of ventilation.

Fig. 11 shows the overpressure history of the four monitoring points (P1, P2, P3, P4) when the hydrogen cloud was ignited 6.1s after the beginning of the hydrogen release. The characteristics of the overpressure were almost the same with those when the hydrogen cloud was ignited 3.1s after release. The comparison of Fig. 10 and Fig. 11 showed that the maximum overpressure increased if ventilation was present. And both the growth rate of the overpressure after ignition and the attenuation rate after reaching the peak increased with the increasing ignition delay time.

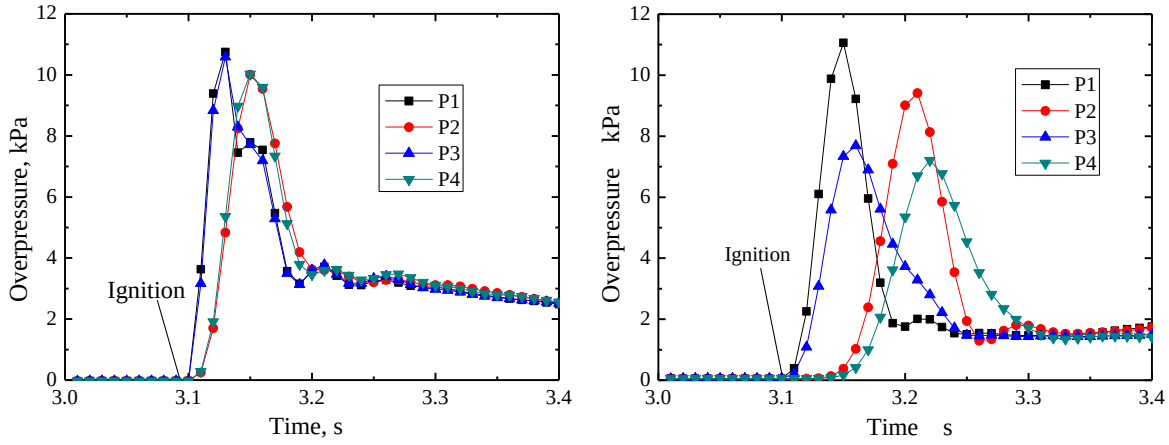

(a) 0m/s (b) 6m/s

Figure 10. Overpressure history when the hydrogen cloud was ignited 3.1s after the beginning of the hydrogen release

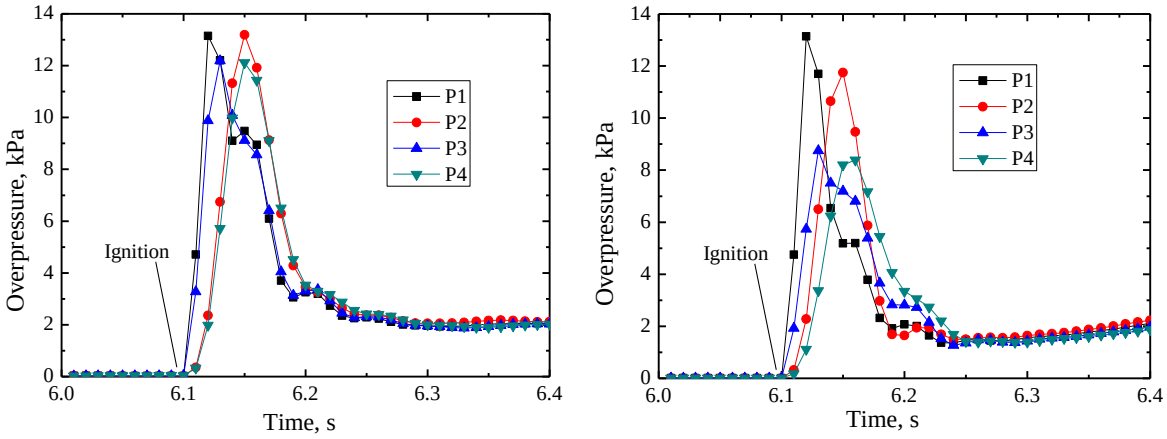

(a) 0m/s (b) 6m/s

Figure 11. Overpressure history when the hydrogen cloud was ignited 6.1s after the beginning of the hydrogen release

5.0 CONCLUSIONS

In this article, the risk associated with hydrogen releases from on-board high-pressure hydrogen vessels in tunnels were analysed using the Partially Averaged Navier-Stokes (PANS) turbulence model. The influences of the tunnel ventilation facilities on the hydrogen flow characteristics and the flammable hydrogen cloud sizes were studied. The tunnel layouts were designed according to the subsea tunnel. And a range of longitudinal ventilation conditions have been considered to investigate the hydrogen releases and the sizes of the flammable gas cloud. It was revealed that ventilation can greatly influence the distribution of hydrogen when hydrogen released from the PRDs. The upstream of the ventilation was less hazardous than the downstream and the risk around the hydrogen leaking vehicle was reduced significantly. Then the hydrogen combustion simulation was carried out after fixed leaking time. The overpressures induced after the ignition of leaking hydrogen were studied. The influences of ventilation and ignition delay time on the overpressure were also investigated. It was concluded that the growth rate of the overpressure after ignition and the attenuation rate after reaching the peak decreased with the increasing of ventilation. While the growth rate of the overpressure after

ignition and the attenuation rate after reaching the peak increased with the increasing ignition delay time.

ACKNOWLEDGEMENTS

This research is funded by the National Natural Science Foundation of China (No. 51306166 and 51206101) and the scientific research foundation of Shandong province Outstanding Young Scientist Award (No: BS2013NJ017).

REFERENCES

1. Veziroglu, T.N., Sahin, S., 21st Century's energy: hydrogen energy system, Energy Conversion and Management, 49, No. 7, 2008, pp. 1820-1831.
2. Molkov, V., Brennan, S., Safety assessment of unignited hydrogen discharge from onboard storage in garages with low levels of natural ventilation, *International Journal of Hydrogen Energy*, **38**, No. 19, 2013, pp. 8159-8166.
3. Houf, W., Schefer, R., Analytical and experimental investigation of small-scale unintended releases of hydrogen, *International Journal of Hydrogen Energy*, **33**, No. 4, 2008, pp. 1435-1444.
4. Takano, K., Okabayashi, K., Kouchi, A., Nonaka, T., Hashiguchi, K. and Chitose, K., Dispersion and explosion field tests for 40MPa pressurized hydrogen, *International Journal of Hydrogen Energy*, **32**, No. 13, 2007, pp. 2144-2153.
5. Ruggles, A.J. and Ekoto, I.W., Experimental investigation of nozzle aspect ratio effects on underexpanded hydrogen jet release characteristics, *International Journal of Hydrogen Energy*, **39**, No. 35, 2014, pp. 20331-20338.
6. Olvera, A.H. and Choudhuri, A.R., Numerical simulation of hydrogen dispersion in the vicinity of a cubical building in stable stratified atmospheres, *International Journal of Hydrogen Energy*, **31**, No. 15, 2006, pp. 2356-2369.
7. Makarov, D. and Molkov, V., Plane hydrogen jets, *International Journal of Hydrogen Energy*, **38**, No. 19, 2013, pp. 8068-8083.
8. Middha, P. and Hansen, O.R., CFD simulation study to investigate the risk from hydrogen vehicles in tunnels, *International Journal of Hydrogen Energy*, **34**, No. 14, 2009, pp. 5875-5886.
9. Molkov, V., Verbecke, F. and Makarov, D., LES of hydrogen-air deflagrations in a 78.5-m tunnel, *Combustion Science and Technology*, **180**, No. 5, 2008, pp. 796-808.
10. Houf, W.G., Evans, G.H., Merilo, E, Groethe, M. and James, S.C., Releases from hydrogen fuel-cell vehicles in tunnels, *International Journal of Hydrogen Energy*, **37**, No. 1, 2012, pp. 715-719.
11. Baraldi, D., Kotchourko, A., Lelyakin, A., Yanez, J., Middha, P., Hansen, O.R., Gavrikov, A., Efimenko, A., Verbecke, F., Makarov, D. and Molkov, V., An inter-comparison exercise on CFD model capabilities to simulate hydrogen deflagrations in a tunnel, *International Journal of Hydrogen Energy*, **34**, No. 18, 2009, pp. 7862-7872.
12. Tolias, I.C., Venetsanos, A.G., Markatos, N. and Kiranoudis, C.T., CFD modeling of hydrogen deflagration in a tunnel, *International Journal of Hydrogen Energy*, **39**, No. 35, 2014, pp. 20538-20546.
13. Girimaji, S.S., Partially-averaged Navier-Stokes model for turbulence: a Reynolds-averaged Navier-Stokes to direct numerical simulation bridging method, *Journal of Applied Mechanics*, **73**, No. 5, 2006, pp. 413-421.
14. Germano, M., Turbulence: The Filtering Approach, *Journal of Fluid Mechanics*, **238**, 1992, pp. 325-336.
15. Versteeg, H.K. and Malalasekera, W., An introduction to computational fluid dynamics: the finite volume method, 1995, Wiley, New York.

16. Chernyavsky, B., Wu, T.C., Peneau, F., Benard, P., Oshkai, P. and Djilali, N., Numerical and experimental investigation of buoyant gas release: Application to hydrogen jets, *International Journal of Hydrogen Energy*, **35**, No. 3, 2011, pp. 2645-2655.
17. Zheng, J.Y., Bie, H.Y., Xu, P., Chen, H.G., Liu, P.F., Xiang, L. and Liu, Y.L., Experimental and numerical studies on the bonfire test of high-pressure hydrogen storage vessels, *International Journal of Hydrogen Energy*, **35**, No. 15, 2010, pp. 8191-8198.